

OPTIMIZED MINIMAL 4D GAUSSIAN SPLATTING

Minseo Lee^{1*} Byeonghyeon Lee^{1*} Lucas Yunkyu Lee^{2,3} Eunsoo Lee⁴
 Sangmin Kim² Seunghyeon Song⁴ Joo Chan Lee⁴ Jong Hwan Ko⁴
 Jaesik Park² Eunbyung Park^{1†}

¹ Yonsei University ² Seoul National University ³ POSTECH ⁴ Sungkyunkwan University

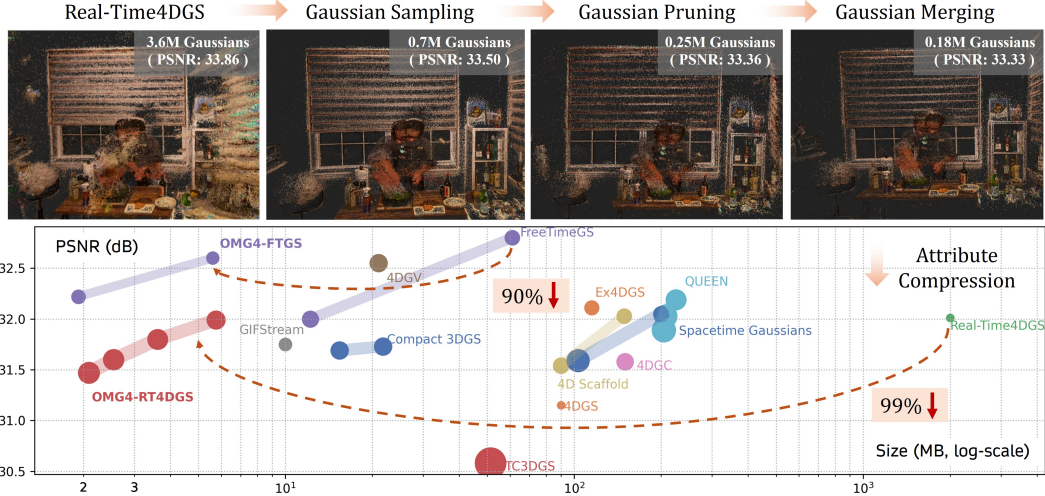


Figure 1: The overall *OMG4* pipeline and performance comparison. *OMG4* is a multi-stage 4DGS compression framework, progressively identifying important Gaussians (*Gaussian Sampling*), pruning unnecessary Gaussians (*Gaussian Pruning*), and merging similar Gaussians (*Gaussian Merging*), followed by attribute compression. The rate-distortion curve shows that *OMG4* achieved significant improvements over recent state-of-the-art methods (larger circles indicate higher FPS).

ABSTRACT

4D Gaussian Splatting has emerged as a new paradigm for dynamic scene representation, enabling real-time rendering of scenes with complex motions. However, it faces a major challenge of storage overhead, as millions of Gaussians are required for high-fidelity reconstruction. While several studies have attempted to alleviate this memory burden, they still face limitations in compression ratio or visual quality. In this work, we present *OMG4* (Optimized Minimal 4D Gaussian Splatting), a framework that constructs a compact set of salient Gaussians capable of faithfully representing 4D Gaussian models. Our method progressively prunes Gaussians in three stages: (1) *Gaussian Sampling* to identify primitives critical to reconstruction fidelity, (2) *Gaussian Pruning* to remove redundancies, and (3) *Gaussian Merging* to fuse primitives with similar characteristics. In addition, we integrate implicit appearance compression and generalize Sub-Vector Quantization (SVQ) to 4D representations, further reducing storage while preserving quality. Extensive experiments on standard benchmark datasets demonstrate that *OMG4* significantly outperforms recent state-of-the-art methods, reducing model sizes by over 60% while maintaining reconstruction quality. These results position *OMG4* as a significant step forward in compact 4D scene representation, opening new possibilities for a wide range of applications. Our source code is available at <https://minshirley.github.io/OMG4/>.

*Equal contribution

†Corresponding author

1 INTRODUCTION

3D Gaussian Splatting (Kerbl et al., 2023) has recently achieved remarkable success, becoming a backbone for diverse 3D vision tasks ranging from 3D novel view synthesis and reconstruction to downstream applications such as visual odometry (Keetha et al., 2024; Yan et al., 2024), 3D scene editing (Wang et al., 2025b; Lee et al., 2025a), and degradation-aware rendering (Lee et al., 2024a; Yu et al., 2024; Wan et al., 2025), to name a few. Building on this success, 4D Gaussian representations that explicitly model space and time have emerged as a new paradigm for dynamic scene reconstruction (Yang et al., 2024; Wu et al., 2024; Yang et al., 2023; Wang et al., 2025a). By augmenting each Gaussian primitive with temporal parameters, these approaches can effectively capture object motion and appearance variations over time, enabling photorealistic novel view synthesis in real time. This capability opens the door to a wide range of applications, such as free-viewpoint video (Girish et al., 2024b; Li et al., 2025; Sun et al., 2024), autonomous driving simulation Khan et al. (2024); Zhou et al. (2024), and VR/AR Pan et al. (2025); Jiang et al. (2024); Xu et al. (2023), where spatio-temporal coherence and real-time rendering are crucial.

Modeling the dynamic scenes using Gaussian primitives has evolved in two directions. Deformation-based methods employ a canonical set of 3D Gaussians and learn a deformation field that predicts per-primitive displacement and maps canonical primitives to each time step (Wu et al., 2024; Yang et al., 2023). The other approach treats the space-time as a single volume and optimizes a set of 4D Gaussian primitives, extending 3D Gaussians to the time axis for temporally varying appearance (Yang et al., 2024). By encoding motions within primitives rather than through warping, it can naturally handle complex non-rigid dynamics and occlusions, yielding higher-fidelity reconstructions.

Nevertheless, current 4D Gaussian representations often carry a substantial computational cost and memory footprint. The number of primitives can grow to millions (e.g., Real-Time4DGS (Yang et al., 2024) produces millions of 4D Gaussians, consuming over a gigabyte of memory), with each primitive carrying high-dimensional attributes that evolve over time. As a result, storage requirements frequently exceed practical limits, particularly under real-time constraints, on mobile devices, or in streaming scenarios. This overhead further complicates various downstream tasks, highlighting the need for effective storage reduction techniques that preserve both visual fidelity and rendering speed.

Several works have attempted to alleviate the significant storage requirement of explicit 4D representations (Yuan et al., 2025; Zhang et al., 2025; Li et al., 2025). 4DGS-1K (Yuan et al., 2025) presents a lifespan-based importance score to prune short-lived Gaussians, reducing the number of primitives and compressing the representation to hundreds of megabytes. GIFStream (Li et al., 2025) performs motion-aware pruning using feature streams and further mitigates storage overhead. On the other hand, Light4GS (Liu et al., 2025) leverages a deep context model, and ADC-GS (Huang et al., 2025) adopts an anchor-based structure and hierarchical approach for modeling motions at various scales to compress a deformation-based approach (e.g., (Wu et al., 2024)). Despite these advances, existing methods still require tens of megabytes to represent only a few seconds of dynamic scenes (e.g., 10 sec in N3DV (Li et al., 2022b)), limiting their practicality for long-duration and high-resolution dynamic contents.

In this paper, we propose *OMG4* (Optimized Minimal 4D Gaussian Splatting), a novel framework designed to reconstruct dynamic scenes with high fidelity and compact model size. Our approach is primarily based on Real-Time4DGS (Yang et al., 2024), which represents a dynamic scene as a 4D volume parameterized by a set of millions of 4D primitives, demanding substantial storage. We introduce a multi-stage optimization pipeline that progressively reduces the number of Gaussians, consisting of *Gaussian Sampling*, *Gaussian Pruning*, and *Gaussian Merging*. Furthermore, we incorporate implicit appearance modeling and generalize the Sub-Vector Quantization (SVQ) framework (Lee et al., 2025b), originally developed for static scenes, to dynamic 4D representations for additional compression.

We begin by analyzing the spatio-temporal properties of each Gaussian through its contribution to the rendered image. This analysis motivates *Gaussian Sampling*, which employs gradient-based scores to capture the impact of Gaussians in both static and dynamic regions, retaining only the salient ones. To further refine the representation, *Gaussian Pruning* eliminates redundant Gaussians, while *Gaussian Merging* leverages inter-Gaussian correlations to identify and fuse Gaussians with

similar attributes, yielding a more compact set of primitives. These steps collectively provide a compact yet expressive Gaussian representation of dynamic scenes. Once we construct a compact Gaussian set through these steps, we encode high-dimensional appearance attributes of Gaussians using a small MLP. We subsequently apply the SVQ that we extend for 4D representation to other attributes, compressing the model size.

We conduct comprehensive experiments on the N3DV (Li et al., 2022b) and MPEG (Li et al., 2025) datasets and evaluate the proposed method under various metrics. To the best of our knowledge, we achieve state-of-the-art performance under a strict memory budget of around 3 MB, significantly reducing the volume of the baseline model by three orders of magnitude. Notably, compared to GIFStream (Li et al., 2025), a recent state-of-the-art approach, our method reduces storage size by approximately 65% (from 10.0 MB to 3.61 MB in the N3DV dataset) while maintaining comparable reconstruction quality. We believe that the proposed approach represents a promising step for the field, opening new avenues for various research directions and practical applications.

To sum up, our contributions are as follows:

- We propose a novel multi-stage framework, progressively reducing the number of Gaussians, *Gaussian Sampling*, *Gaussian Pruning*, and *Gaussian Merging*, while maintaining the reconstruction quality.
- We generalize Sub-Vector Quantization (SVQ) for 4D representations together with implicit appearance compression, enabling highly compact yet high-fidelity models.
- To the best of our knowledge, we achieve state-of-the-art performance around a 3 MB memory budget, and negligible visual quality loss compared to the baseline model while condensing the model size from gigabytes to a few megabytes.

2 RELATED WORK

2.1 3D GAUSSIAN SPLATTING AND COMPRESSION

3D Gaussian Splatting (3DGS) (Kerbl et al., 2023) enables high-fidelity scene reconstruction with real-time rendering, using 3D Gaussians as fundamental primitives. However, it typically requires millions of primitives, which incurs substantial memory costs, urging the need for effective compression solutions. Several studies (Fan et al., 2024; Girish et al., 2024a; Shin et al., 2025; Lee et al., 2024c; 2025b) have proposed primitive pruning and attribute compression. LocoGS (Shin et al., 2025) proposes a locality-aware compact representation that encodes locally coherent Gaussian attributes with a multi-scale hash grid. Compact 3DGS (Lee et al., 2024c) adopts a learnable mask to remove unnecessary Gaussians and vector quantization (VQ) to condense geometry attributes. OMG (Lee et al., 2025b) further aims for a more compact representation, introducing sub-vector quantization (SVQ) that splits the vectors into multiple small sub-vectors and applies VQ, achieving significant performance improvement. Other works, on the other hand, present anchor-based approaches to address Gaussian redundancy (Lu et al., 2023; Chen et al., 2024). Scaffold-GS (Lu et al., 2023) organizes local Gaussians around the learned anchor points and predicts their attributes with lightweight MLPs, while HAC (Chen et al., 2024) leverages a hash grid to capture spatial consistencies among the anchors. Although these approaches effectively reduce the storage requirements of 3DGS, they do not straightforwardly generalize to 4D representations.

2.2 DYNAMIC 3D GAUSSIAN SPLATTING AND COMPRESSION

Early efforts to extend static scene reconstruction to dynamic settings (Cao & Johnson, 2023; Fridovich-Keil et al., 2023; Wang et al., 2023; Pumarola et al., 2020; Li et al., 2022a) were primarily based on neural volumetric rendering, but suffered from high computational costs. More recently, many studies have sought to extend 3DGS to dynamic scenes, which can be broadly categorized into two approaches: (1) representing dynamic scenes with 4D Gaussian primitives that jointly encode spatial and temporal dimensions (Yang et al., 2024; Li et al., 2024), or (2) deforming 3D Gaussians at each timestamp via a deformation field (Kratimenos et al., 2024; Bae et al., 2024; Wu et al., 2024; Yang et al., 2023). Among them, Real-Time4DGS (Yang et al., 2024) achieves high-fidelity modeling of dynamic scenes by parameterizing the 4D volume with a set of 4D Gaussians. Most recently,

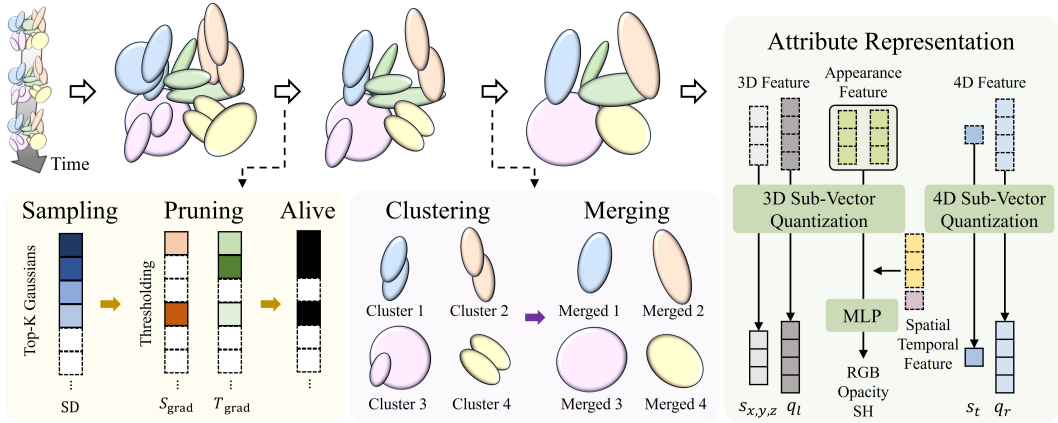


Figure 2: The overall architecture of the proposed *OMG4*.

FreeTimeGS (Wang et al., 2025a) has shown promising performance by moving 3D Gaussians over time, leveraging motion vectors.

Similar to 3DGS, dynamic extensions also require a significant number of primitives, motivating the development of lightweight methods. Within the first category, which employs 4D Gaussian primitives, CSTG (Lee et al., 2024b), MEGA (Zhang et al., 2025), and 4DGS-1K (Yuan et al., 2025) have been proposed. Among them, 4DGS-1K (Yuan et al., 2025) reduces storage by discarding Gaussians with short lifespans, achieving a model size of around 50 MB after post-processing. In contrast, other works (Liu et al., 2025; Huang et al., 2025; Chen et al., 2025; Li et al., 2025) focus on compressing deformable 3DGS. In this paper, we primarily target Real-Time4DGS (Yang et al., 2024), which demands an extremely large number of primitives (approximately 2 GB per scene), and aim to drastically reduce its memory footprint while preserving its strength in photorealistic dynamic scene reconstruction.

3 PRELIMINARY

Our framework is primarily built upon Real-Time4DGS (Yang et al., 2024)¹, which treats a dynamic scene as a 4D volume, parameterized with a set of 4D Gaussian primitives defined by a 4D mean at spatio-temporal space, an anisotropic 4D covariance, an opacity, and spherical harmonics (SH) coefficients. During rendering, 4D Gaussians are conditioned at timestamp t , yielding 3D position and covariance. For further details, please refer to the original paper.

We denote the set of Gaussians of pretrained Real-Time4DGS model by $\mathcal{P} = \{(x_i, f_i, a_i)\}_{i=1}^N$, where x_i is a spatial mean (i.e., $\mu_{1:3}$), $f_i \in \mathbb{R}^3$ is the zero-th order of the SH coefficient, and a_i denotes the remaining per-primitive attributes such as opacity, scale, and rotation.

4 METHODS

We propose a novel framework for high-fidelity dynamic scene representation with a minimal number of Gaussians consisting of Gaussian Sampling (Sec. 4.1), Gaussian Pruning (Sec. 4.2), Gaussian Merging (Sec. 4.3), and Gaussian attributes compression (Sec. 4.4). An overview of the entire pipeline is provided in Fig. 2.

4.1 GAUSSIAN SAMPLING

Prior methods typically rely on an excessive number of Gaussians for high-quality dynamic scene reconstruction, incurring significant storage overhead. Although recent studies observed that many Gaussians contribute only marginally to reconstruction quality, this challenge has yet to be fully addressed. In this section, we propose the Static-Dynamic Score (SD-Score), which combines a

¹We also applied *OMG* to the recently proposed FreeTimeGS (Wang et al., 2025a). Due to space limits, we are unable to provide the details and kindly refer to the original paper for a full description.



Figure 3: A comparison of rendered images. (Left) Real-Time4DGS (Yang et al., 2024) with 3.6M Gaussians. (Right) 1K optimization after Gaussian Sampling with 0.7M Gaussians.

Static Score and a Dynamic Score to quantify each Gaussian’s contribution. Static regions are often characterized by temporally persistent and spatially dispersed Gaussians, whereas dynamic regions tend to contain temporally short-lived and spatially concentrated Gaussians. Exploiting these properties, our method identifies the salient Gaussians, as shown in Fig. 3, retaining only 20% of those from a pre-trained Real-Time4DGS model (Yang et al., 2024) is sufficient to reconstruct the scene with negligible quality loss.

SD Score. The proposed Static–Dynamic Score (SD-Score) to calculate the importance of each Gaussian is defined as follows:

$$SD^{(i)} = S_{\text{grad}}^{(i)} \cdot T_{\text{grad}}^{(i)}, \quad S_{\text{grad}}^{(i)} = \sum_{j=1}^N \|\nabla_{u_{i,j}} L_j\|_2, \quad T_{\text{grad}}^{(i)} = \sum_{j=1}^N \nabla_{t_i} L_j, \quad (1)$$

where N is the number of input images (# of input views \times # of frames), i is the Gaussian index, L_j is the reconstruction loss of the input image j , $u_{i,j} \in \mathbb{R}^2$ denotes the projected 2D coordinate of the i -th Gaussian for the j -th image, and $t_i \in \mathbb{R}$ is the time coordinate of i -th Gaussian.

Static Score. The static score for the i -th Gaussian, $S_{\text{grad}}^{(i)}$, is defined as an accumulation of the view-space gradients across all timesteps, capturing the overall rendering sensitivity with respect to the Gaussian’s projected coordinates. In static regions, Gaussians are temporally long-lived yet relatively sparse (i.e., fewer Gaussians per unit area), so even small positional perturbations can influence the rendering loss across many timesteps, yielding higher static scores. In contrast, Gaussians associated with dynamic regions are often active only at specific time steps and are spatially dense (e.g., a larger number of Gaussians per unit area). Consequently, the effect of a single Gaussian’s positional change on the overall reconstruction loss is diluted, resulting in lower static scores.

Dynamic Score. The dynamic score for the i -th Gaussian, $T_{\text{grad}}^{(i)}$, is a sum of time gradients that measures the sensitivity of the reconstruction loss with respect to the time coordinate of each Gaussian. Gaussians with a high dynamic Score often imply that they play a pivotal role in representing dynamic regions, as these areas are sensitive to temporal changes, capturing the motion of the objects. We accumulate the signed time gradients rather than their magnitudes to capture consistent temporal trends. This avoids assigning high scores to Gaussians with frequent sign flips (i.e., flickering), enhancing the robustness of the score.

By combining the complementary Static and Dynamic Score, the SD-Score can provide a balanced evaluation of the overall contribution of each Gaussian. We subsequently sample the Gaussians with high SD values with a sampling ratio of τ_{GS} , forming a set of sampled Gaussians, \mathcal{P}_{GS} , and optimize it for T_{GS} iterations.

4.2 GAUSSIAN PRUNING

While the first Gaussian sampling stage with the SD-Score yields a set of critical Gaussians, \mathcal{P}_{GS} , it may still include redundant Gaussians. In response, we introduce a Gaussian Pruning strategy that further refines the set by eliminating superfluous Gaussians that remain after the first stage.

Fig. 4 illustrates the space defined by S_{grad} and T_{grad} , where the curve $T_{\text{grad}} = c/S_{\text{grad}}$ denotes the selection boundary from the first Gaussian sampling stage. Within this space, we identify Gaussians



Figure 4: Illustration of *Gaussian Pruning*. (Left) Space defined by Static and Dynamic score and *Gaussian Sampling Boundary*. (Middle) A rendered image with unique Gaussians that satisfy both unique static and dynamic thresholds, and one after 1K optimization. (Right) A rendered image with redundant Gaussians that are not included in a unique area.

that are likely redundant, and our empirical analysis shows that those with both $S_{\text{grad}}^{(i)}$ and $T_{\text{grad}}^{(i)}$ values being small can be safely filtered out (gray regions in Fig. 4). To this end, we apply thresholding to both scores, with each threshold defined as follows:

$$\mathcal{P}_{GP} = \{G_i \in \mathcal{P}_{GS} \mid (S_{\text{grad}}^{(i)} \geq \tau_S) \vee (T_{\text{grad}}^{(i)} \geq \tau_T)\}, \quad \tau_S = Q_p(\{S_{\text{grad}}^{(i)}\}), \quad \tau_T = Q_p(\{T_{\text{grad}}^{(i)}\}), \quad (2)$$

where τ_S and τ_T are the thresholds for S_{grad} and T_{grad} respectively, and $Q_p(\cdot)$ denotes the p -quantile value, reflecting the relative distribution of Gaussians. As shown in Fig. 4, the pruned set, \mathcal{P}_{GP} , can still represent the scene with fine details and we optimize \mathcal{P}_{GP} for T_{GP} iterations.

One may question the necessity of employing two distinct stages, since, in principle, sampling and pruning could be integrated into a single process. Nevertheless, our experiments indicate that separating these stages proves to be more effective, as evidenced by the ablation study in Sec. 5.2. We hypothesize that this advantage arises from the intermediate optimization performed between the two stages, which further refines the representation and ultimately results in a more compact set.

4.3 GAUSSIAN MERGING

The first two stages, Gaussian Sampling and Gaussian Pruning, are effective in preserving a compact and salient set of Gaussians. However, both stages evaluate the importance of each Gaussian individually, without considering similarities across Gaussians. To further reduce redundancy, we introduce a Gaussian Merging technique that clusters highly similar Gaussians and fuses them into single representative Gaussians.

Gaussian Clustering. We define a Similarity Score to quantify the similarity among Gaussians and identify clusters. We first divide space into a 4D grid and compute the Similarity Score among the Gaussians within the same grid cell. Such a spatio-temporal grid can group Gaussians with temporal proximity, preventing the merging of temporally mismatched Gaussians and preserving temporal coherence, while reducing computational complexity. We define the Similarity Score $S(G_i, G_j)$ between two Gaussians as a sum of spatial proximity and appearance similarity:

$$S(G_i, G_j) = -\|x_i - x_j\|_2^2 + \lambda \|f_i - f_j\|_2^2, \quad (3)$$

where λ is a fixed balancing weight, $x_i \in \mathbb{R}^3$ is the position, and $f_i \in \mathbb{R}^3$ is the zero-th order spherical-harmonics (RGB) coefficient of G_i . A higher score indicates a greater spatial-appearance similarity. For each Gaussian G_i , we construct a cluster of Gaussians C_i by thresholding the Similarity Score with τ_{sim} :

$$C_i = \{i\} \cup \{j \in \mathcal{P}_i \mid S(G_i, G_j) \geq \tau_{\text{sim}}\}, \quad (4)$$

where \mathcal{P}_i denotes a set of Gaussian indices within the spatio-temporal grid cell that contain the Gaussian G_i . We then deduplicate identical clusters and remove subset ones, yielding a final set of maximal clusters, $\mathcal{C} = \{C_q\}_{q=1}^{N_C}$. Gaussians not included in any clusters remain as singletons.

Gaussian Merging. Within each cluster, we assign learnable per-Gaussian weights $w_i^x \in \mathbb{R}$ and $w_i^f \in \mathbb{R}$ to the position and appearance attributes, respectively. During training-time rendering, all

Gaussians in a cluster C_q are replaced by a single proxy whose elements are defined as follows:

$$\bar{x}_q = \sum_{i \in C_q} w_i^x x_i, \quad \bar{f}_q = \sum_{i \in C_q} w_i^f f_i, \quad \bar{a}_q = a_{r(C_q)}, \quad r(C_q) = \arg \max_{i \in C_q} w_i^x, \quad (5)$$

where the both weights w_i^x, w_i^f are normalized per cluster. The position and appearance are the weighted sum of the Gaussians within the cluster, and the attributes of the representative Gaussian is used for \bar{a}_q . We optimize both weights w_i^x, w_i^f for T_{GM} iterations and repeat the Gaussian Merging M times, progressively increasing the grid size. The detailed process of Gaussian Merging is provided in appendix A.3.

4.4 ATTRIBUTE COMPRESSION

Given the compact Gaussian set, we compress attributes by adapting the OMG architecture (Lee et al., 2025b), which is initially designed for static 3DGS, to the 4DGS setting with explicit time conditioning. Concretely, we follow OMG’s compression pipeline, which employs an MLP to extract spatial features and three additional small MLPs that take the spatial features and position as inputs, producing opacities, static colors, and view-dependent colors, respectively. We extend these MLPs to also take the time coordinate, enabling time-varying opacity and appearance.

Furthermore, OMG introduced Sub-Vector Quantization (SVQ), which partitions an input vector into sub-vectors and quantizes each with a small codebook, demonstrating both high efficiency and reconstruction quality. In this work, we extend SVQ to dynamic 3D scene representations. Specifically, we retain the 4D Gaussian means in full precision for stability, while applying SVQ to other attributes, including the additional rotation quaternion and temporal-axis scales introduced in Real-Time4DGS (Yang et al., 2024) to model scene motion. However, quantizing both static and dynamic attributes simultaneously leads to unstable optimization. To mitigate this, we propose a staged SVQ scheme: SVQ is first applied only to 3D attributes and optimized for T_{3D} iterations, after which SVQ is activated for 4D attributes. This staged approach decouples temporal and appearance sensitivities from static components, resulting in stable optimization. Finally, we compress the quantized elements using Huffman encoding (Huffman, 1952) followed by LZMA compression (Pavlov).

5 EXPERIMENTS AND RESULTS

5.1 IMPLEMENTATION DETAILS

For each stage, we optimize for 1,000 iterations ($T_{GS} = T_{GP} = T_{GM} = 1,000$). Starting from a pretrained model, we first perform *Gaussian Sampling*, followed by *Gaussian Pruning* at the 1,000th iteration. *Gaussian Merging* is then applied twice, at the 2,000th and 3,000th iterations, respectively. After merging, attribute compression begins. We train the MLPs at the 4,000th iteration and keep training until the end. We start applying SVQ to 3D attributes at the 9,000th iteration, and then SVQ to 4D attributes at the 10,000th iteration. For the medium-size model (*Ours-M*), the sampling ratio is set to $\tau_{GS} = 0.2$, and a 0.8-quantile threshold is used for *Gaussian Pruning*. We perform *Gaussian Merging* twice, increasing the spatial grid size by a factor of 1.2, while keeping a constant temporal grid size of 2.0. We used all identical hyperparameters across the dataset. Learning rates, codebook sizes, and other hyperparameters follow Real-Time4DGS (Yang et al., 2024) and OMG (Lee et al., 2025b). All experiments are conducted on a single RTX 3090 GPU.

5.2 RESULTS AND ANALYSIS

We conduct experiments on N3DV (Li et al., 2022b) and *Bartender* data² of the MPEG (Li et al., 2025) dataset. As shown in Tab. 1 and Fig. 5, we effectively reduce the model size of the baseline Real-Time4DGS (Yang et al., 2024), from 2 GB to around 3 MB, while preserving comparable visual quality (*Ours-M*). Notably, *OMG4* can reduce the storage requirement of the original Real-Time4DGS (Yang et al., 2024) by **99%**. In addition, compared to a recent state-of-the-art method GIFStream (Li et al., 2025), *OMG4* achieved **65%** reduction in storage (from 10 MB to 3.61 MB) while even improving the PSNR (31.75 vs. 31.80). By slightly increasing the model size (from 3.61

²Other data from the MPEG dataset were not publicly available.

Table 1: Quantitative results on N3DV (Li et al., 2022b) dataset. All results without * mark are sourced from the original paper. † denotes post-processed models. • denotes the results excluding *Coffee Martini* scene.

Method	PSNR↑	SSIM↑	LPIPS↓	FPS↑	# Gaussians↓	Storage (MB)↓
1352 × 1014 Resolution						
K-Planes (Fridovich-Keil et al., 2023)	31.63	-	-	0.3	-	311
HexPlane (Cao & Johnson, 2023)•	31.71	-	0.075	0.2	-	250
Real-Time4DGS (Yang et al., 2024)*	31.96	0.946	0.051	57	3,397,510	2087
STG (Li et al., 2024)	32.05	0.946	0.044	140	-	200
4DGS (Wu et al., 2024)	31.15	-	0.049	82	-	18
MEGA (Zhang et al., 2025)	31.49	-	0.057	77	-	25.05
CSTG (Lee et al., 2024b)†	31.69	0.945	0.054	186	-	15.4
GIFStream (Li et al., 2025)	31.75	0.938	0.051	95	-	10.0
ADC-GS (Huang et al., 2025)•-L	31.67	-	0.061	110	-	6.57
ADC-GS (Huang et al., 2025)•-S	31.41	-	0.066	126	-	4.04
Ours-L	31.99	0.943	0.056	202	283,297	5.75
Ours-M	31.80	0.941	0.059	246	171,136	3.61
Ours-S	31.60	0.939	0.064	258	137,414	2.54
Ours-T	31.47	0.937	0.067	275	111,402	2.09
Ours•-L	32.68	0.949	0.051	188	264,073	5.40
Ours•-T	32.19	0.944	0.067	283	103,301	1.96
1024 × 768 Resolution						
Real-Time4DGS (Yang et al., 2024)*	32.21	0.950	0.040	96	2,770,350	1701
4DGS-1K (Yuan et al., 2025)†	31.87	0.944	0.053	805	666,632	49.50
Light4GS (Liu et al., 2025)•-L	31.69	-	0.053	37	-	5.46
Light4GS (Liu et al., 2025)•-S	31.48	-	0.064	40	-	3.77
Ours-L	32.28	0.948	0.043	189	247,707	5.08
Ours-M	32.09	0.946	0.047	253	147,153	3.15
Ours-S	31.81	0.944	0.051	246	120,513	2.25
Ours-T	31.75	0.942	0.053	302	96,942	1.85
Ours•-L	32.80	0.951	0.044	192	139,320	2.99
Ours•-T	32.58	0.950	0.047	308	113,862	2.13

Table 2: Quantitative results on *Bartender* scene of MPEG (Li et al., 2025) dataset. All results without * mark are sourced from the original paper.

Method	PSNR↑	SSIM↑	LPIPS (VGG)↓	FPS↑	# Gaussians↓	Storage (MB)↓
Real-Time4DGS (Yang et al., 2024)*	32.44	0.895	0.1579	115	2,653,870	1630
GIFStream (Li et al., 2025)-L	31.94	0.879	0.190	-	-	5.3
GIFStream (Li et al., 2025)-S	31.35	0.872	0.207	-	-	2.3
Ours-L	32.19	0.892	0.175	203	319,906	6.33
Ours-S	31.91	0.887	0.190	238	196,319	4.00

Table 3: Quantitative results on applying *OMG4* to FTGS (FreeTimeGS) (Wang et al., 2025a), evaluated on N3DV (Li et al., 2022b) dataset (*We reproduced FTGS models since the codes and pretrain models are not publicly available).

Method	PSNR↑	SSIM↑	LPIPS↓	FPS↑	# Gaussians↓	Storage (MB)↓
FTGS-L*	32.80	0.9579	0.0398	129	500,000	61.04
FTGS-S*	32.00	0.9504	0.0559	160	100,000	12.21
Ours (FTGS-L, AC Only)	32.59	0.9568	0.0405	73	500,000	9.66
Ours (FTGS-S, AC Only)	32.15	0.9496	0.0551	107	100,000	2.12
Ours (FTGS-L)	32.62	0.9562	0.0411	91	283,977	5.60
Ours (FTGS-S)	32.22	0.9516	0.0491	112	90,227	1.92

MB to 5.08 MB, *Ours-L*), *OMG4* could even outperform the baseline Real-Time4DGS (Yang et al., 2024).

4DGS-1K (Yuan et al., 2025) achieves the highest FPS due to its visibility mask, which identifies the visible Gaussians at a given timestamp t , and only those Gaussians are involved in rasterization, thereby dramatically reducing computational costs. Although we do not employ any visibility masks, as improving FPS is outside our scope, we can still improve the FPS of the baseline model by $4.31\times$, thanks to our compact representation. We additionally conduct experiments on *Bartender* data of the MPEG (Li et al., 2025) dataset, which exhibits significantly more complex motions than



Figure 5: Qualitative results on N3DV dataset (Li et al., 2022b).

Table 4: Ablation study on each module of the proposed method where *GS*, *GP*, *GM*, *AC* refers to *Gaussian Sampling*, *Gaussian Pruning*, *Gaussian Merging* and *Attribution Compression*, respectively. *GS+GP* means applying *GS* and *GP* simultaneously at the first iteration.

GS+GP	Modules					PSNR \uparrow	SSIM \uparrow	LPIPS \downarrow	FPS \uparrow	# Gaussians \uparrow	Storage (MB) \downarrow
	GS	GP	GM	AC	AC						
						31.96	0.9459	0.0506	57	3,397,510	2126
				✓		OOM					
	✓			✓		32.07	0.9454	0.0518	126	679,502	13.26
	✓	✓		✓		31.89	0.9429	0.0559	244	235,027	4.83
✓			✓	✓		31.68	0.9407	0.0606	217	171,214	3.61
	✓	✓	✓	✓		31.80	0.9414	0.0594	246	171,136	3.61

the N3DV (Li et al., 2022b) dataset. Following GIFStream (Li et al., 2025), we use the first 65 frames for our experiment. *OMG4* consistently outperforms the state-of-the-art methods, efficiently reconstructing the scene with minimal storage overhead, as reported in Tab. 2.

Application on FreeTimeGS. We further extend *OMG4* to FreeTimeGS (Wang et al., 2025a), comprehensively evaluating the proposed method beyond Real-Time4DGS (Yang et al., 2024). We begin with the pretrained FreeTimeGS models³ with 500K Gaussians (FTGS-L) as our backbone model and apply *OMG4*, progressively pruning Gaussians from 500K to around 280K (Ours (FTGS-L)) and 90K (Ours (FTGS-S)) primitives. To see the effectiveness of the proposed multi-stage frameworks, we also provided the results of Ours (FTGS-L, AC only) and Ours (FTGS-L, AC only), where we apply only the proposed attribute compression technique to the pretrained FreeTimeGS models (FTGS-L: 500K Gaussians, FTGS-S: 100K Gaussians). As Tab. 3 shows, *OMG4* can significantly reduce the storage of FreeTimeGS by **90%**. Even under the stricter memory budget of around 2 MB, *OMG4* still remains effective, benefiting from its prior. This result highlights the versatility of *OMG4*, showing that it can be effectively applied to diverse 4D representation methods.

Ablation Studies. In this section, we present ablation studies on each module of *OMG4*, summarized in Tab. 4. First, directly applying *Attribute Compression* to Real-Time4DGS (Yang et al., 2024) incurs out-of-memory failure, due to a larger number of Gaussians. When we implement *Gaussian Sampling* only, we can remove 80% of Gaussians, even outperforming Real-Time4DGS. We assume this is because *Gaussian Sampling* can act as a regularizer by eliminating noisy Gaussians, hence raising visual quality. Adding *Gaussian Pruning* can reduce the memory footprint from gigabytes to a few megabytes, and *Gaussian Merging* achieves the minimal number of Gaussians, integrating highly correlated Gaussians. It may appear possible to perform *Gaussian Sampling* and *Gaussian Pruning* simultaneously. However, our ablation study (fifth row, *GS+GP* in Tab. 4) shows that doing so results in a PSNR drop of 0.12 dB. This finding highlights the importance of the proposed multi-stage pipeline: by first stabilizing the optimization with *Gaussian Sampling* and then progressively reducing the number of Gaussians through *Gaussian Pruning*, we are able to maintain reconstruction quality while ensuring stable training. One possible explanation is that T_{GS} iteration training before *Gaussian Pruning* stabilizes the whole optimization process. Therefore, our pipeline separates *Gaussian Sampling* and *Gaussian Pruning* with a sufficient optimization term.

³We reproduced FreeTimeGS models since the codes and pre-trained models are not publicly available.

6 CONCLUSION

We introduce *OMG4*, a compact dynamic-scene representation that progressively reduces the number of primitives and compresses the Gaussian attributes. We present *Gaussian Sampling* and *Gaussian Pruning*, which reduce the number of Gaussians significantly and further leverage the correlation of Gaussians to fuse the similar Gaussians in the *Gaussian Merging* stage. Lastly, we couple these Gaussian minimization techniques with implicit appearance encoding and 4D extension of Sub-Vector Quantization (SVQ). Consequently, *OMG4* compresses Real-Time4DGS by three orders of magnitude at comparable fidelity. *OMG4* also transfers to the recent state-of-the-art method, FreeTimeGS, achieving 90% storage reduction while maintaining high reconstruction quality. With its significant performance improvement, we believe *OMG4* marks an important advance in 4D scene representation, opening new opportunities for research and various practical applications.

REFERENCES

- Jeongmin Bae, Seoha Kim, Youngsik Yun, Hahyun Lee, Gun Bang, and Youngjung Uh. Per-gaussian embedding-based deformation for deformable 3d gaussian splatting, 2024. URL <https://arxiv.org/abs/2404.03613>.
- Ang Cao and Justin Johnson. Hexplane: A fast representation for dynamic scenes, 2023. URL <https://arxiv.org/abs/2301.09632>.
- Yihang Chen, Qianyi Wu, Weiyao Lin, Mehrtash Harandi, and Jianfei Cai. Hac: Hash-grid assisted context for 3d gaussian splatting compression, 2024. URL <https://arxiv.org/abs/2403.14530>.
- Zicong Chen, Zhenghao Chen, Wei Jiang, Wei Wang, Lei Liu, and Dong Xu. 4dgs-cc: A contextual coding framework for 4d gaussian splatting data compression, 2025. URL <https://arxiv.org/abs/2504.18925>.
- Zhiwen Fan, Kevin Wang, Kairun Wen, Zehao Zhu, Dejie Xu, and Zhangyang Wang. Lightgaussian: Unbounded 3d gaussian compression with 15x reduction and 200+ fps, 2024. URL <https://arxiv.org/abs/2311.17245>.
- Sara Fridovich-Keil, Giacomo Meanti, Frederik Warburg, Benjamin Recht, and Angjoo Kanazawa. K-planes: Explicit radiance fields in space, time, and appearance, 2023. URL <https://arxiv.org/abs/2301.10241>.
- Sharath Girish, Kamal Gupta, and Abhinav Shrivastava. Eagles: Efficient accelerated 3d gaussians with lightweight encodings, 2024a. URL <https://arxiv.org/abs/2312.04564>.
- Sharath Girish, Tianye Li, Amrita Mazumdar, Abhinav Shrivastava, David Luebke, and Shalini De Mello. Queen: Quantized efficient encoding of dynamic gaussians for streaming free-viewpoint videos, 2024b. URL <https://arxiv.org/abs/2412.04469>.
- He Huang, Qi Yang, Mufan Liu, Yiling Xu, and Zhu Li. Adc-gs: Anchor-driven deformable and compressed gaussian splatting for dynamic scene reconstruction, 2025. URL <https://arxiv.org/abs/2505.08196>.
- David A Huffman. A method for the construction of minimum-redundancy codes. *Proceedings of the IRE*, 40(9):1098–1101, 1952.
- Ying Jiang, Chang Yu, Tianyi Xie, Xuan Li, Yutao Feng, Huamin Wang, Minchen Li, Henry Lau, Feng Gao, Yin Yang, et al. Vr-gs: A physical dynamics-aware interactive gaussian splatting system in virtual reality. In *ACM SIGGRAPH 2024 Conference Papers*, pp. 1–1, 2024.
- Nikhil Keetha, Jay Karhade, Krishna Murthy Jatavallabhula, Gengshan Yang, Sebastian Scherer, Deva Ramanan, and Jonathon Luiten. Splatam: Splat track & map 3d gaussians for dense rgb-d slam. In *Proceedings of the IEEE/CVF Conference on Computer Vision and Pattern Recognition*, pp. 21357–21366, 2024.

-
- Bernhard Kerbl, Georgios Kopanas, Thomas Leimkühler, and George Drettakis. 3d gaussian splatting for real-time radiance field rendering, 2023. URL <https://arxiv.org/abs/2308.04079>.
- Mustafa Khan, Hamidreza Fazlali, Dhruv Sharma, Tongtong Cao, Dongfeng Bai, Yuan Ren, and Bingbing Liu. Autosplat: Constrained gaussian splatting for autonomous driving scene reconstruction, 2024. URL <https://arxiv.org/abs/2407.02598>.
- Agelos Kratimenos, Jiahui Lei, and Kostas Daniilidis. Dynmf: Neural motion factorization for real-time dynamic view synthesis with 3d gaussian splatting, 2024. URL <https://arxiv.org/abs/2312.00112>.
- Byeonghyeon Lee, Howoong Lee, Xiangyu Sun, Usman Ali, and Eunbyung Park. Deblurring 3d gaussian splatting. In *European Conference on Computer Vision*, pp. 127–143. Springer, 2024a.
- Dong In Lee, Hyeongcheol Park, Jiyoung Seo, Eunbyung Park, Hyunje Park, Ha Dam Baek, Sangheon Shin, Sangmin Kim, and Sangpil Kim. Editsplat: Multi-view fusion and attention-guided optimization for view-consistent 3d scene editing with 3d gaussian splatting, 2025a. URL <https://arxiv.org/abs/2412.11520>.
- Joo Chan Lee, Daniel Rho, Xiangyu Sun, Jong Hwan Ko, and Eunbyung Park. Compact 3d gaussian splatting for static and dynamic radiance fields, 2024b. URL <https://arxiv.org/abs/2408.03822>.
- Joo Chan Lee, Daniel Rho, Xiangyu Sun, Jong Hwan Ko, and Eunbyung Park. Compact 3d gaussian representation for radiance field, 2024c. URL <https://arxiv.org/abs/2311.13681>.
- Joo Chan Lee, Jong Hwan Ko, and Eunbyung Park. Optimized minimal 3d gaussian splatting, 2025b. URL <https://arxiv.org/abs/2503.16924>.
- Hao Li, Sicheng Li, Xiang Gao, Abudouaihati Batuer, Lu Yu, and Yiyi Liao. Gifstream: 4d gaussian-based immersive video with feature stream, 2025. URL <https://arxiv.org/abs/2505.07539>.
- Tianye Li, Mira Slavcheva, Michael Zollhoefer, Simon Green, Christoph Lassner, Changil Kim, Tanner Schmidt, Steven Lovegrove, Michael Goesele, Richard Newcombe, and Zhaoyang Lv. Neural 3d video synthesis from multi-view video, 2022a. URL <https://arxiv.org/abs/2103.02597>.
- Tianye Li, Mira Slavcheva, Michael Zollhoefer, Simon Green, Christoph Lassner, Changil Kim, Tanner Schmidt, Steven Lovegrove, Michael Goesele, Richard Newcombe, et al. Neural 3d video synthesis from multi-view video. In *Proceedings of the IEEE/CVF conference on computer vision and pattern recognition*, pp. 5521–5531, 2022b.
- Zhan Li, Zhang Chen, Zhong Li, and Yi Xu. Spacetime gaussian feature splatting for real-time dynamic view synthesis, 2024. URL <https://arxiv.org/abs/2312.16812>.
- Mufan Liu, Qi Yang, He Huang, Wenjie Huang, Zhenlong Yuan, Zhu Li, and Yiling Xu. Light4gs: Lightweight compact 4d gaussian splatting generation via context model, 2025. URL <https://arxiv.org/abs/2503.13948>.
- Tao Lu, Mulin Yu, Linning Xu, Yuanbo Xiangli, Limin Wang, Dahua Lin, and Bo Dai. Scaffoldgs: Structured 3d gaussians for view-adaptive rendering, 2023. URL <https://arxiv.org/abs/2312.00109>.
- Seungjun Oh, Younggeun Lee, Hyejin Jeon, and Eunbyung Park. Hybrid 3d-4d gaussian splatting for fast dynamic scene representation, 2025. URL <https://arxiv.org/abs/2505.13215>.
- Zipeng Pan, Yuan Zhang, and Tao Lin. Telegs: End-to-end monocular gaussian head for immersive telepresence. In *Proceedings of the 3rd Workshop on Emerging Multimedia Systems*, pp. 37–42, 2025.
- Igor Pavlov. Lzma compression algorithm. <https://www.7-zip.org/sdk.html>.

-
- Albert Pumarola, Enric Corona, Gerard Pons-Moll, and Francesc Moreno-Noguer. D-nerf: Neural radiance fields for dynamic scenes, 2020. URL <https://arxiv.org/abs/2011.13961>.
- Seungjoo Shin, Jaesik Park, and Sunghyun Cho. Locality-aware gaussian compression for fast and high-quality rendering, 2025. URL <https://arxiv.org/abs/2501.05757>.
- Jiakai Sun, Han Jiao, Guangyuan Li, Zhanjie Zhang, Lei Zhao, and Wei Xing. 3dstream: On-the-fly training of 3d gaussians for efficient streaming of photo-realistic free-viewpoint videos, 2024. URL <https://arxiv.org/abs/2403.01444>.
- Yecong Wan, Mingwen Shao, Yuanshuo Cheng, and Wangmeng Zuo. S2gaussian: Sparse-view super-resolution 3d gaussian splatting. In *Proceedings of the Computer Vision and Pattern Recognition Conference*, pp. 711–721, 2025.
- Feng Wang, Sinan Tan, Xinghang Li, Zeyue Tian, Yafei Song, and Huaping Liu. Mixed neural voxels for fast multi-view video synthesis, 2023. URL <https://arxiv.org/abs/2212.00190>.
- Yifan Wang, Peishan Yang, Zhen Xu, Jiaming Sun, Zhanhua Zhang, Yong Chen, Hujun Bao, Sida Peng, and Xiaowei Zhou. Freetimegs: Free gaussian primitives at anytime and anywhere for dynamic scene reconstruction, 2025a. URL <https://arxiv.org/abs/2506.05348>.
- Yuxuan Wang, Xuanyu Yi, Zike Wu, Na Zhao, Long Chen, and Hanwang Zhang. View-consistent 3d editing with gaussian splatting, 2025b. URL <https://arxiv.org/abs/2403.11868>.
- Guanjun Wu, Taoran Yi, Jiemin Fang, Lingxi Xie, Xiaopeng Zhang, Wei Wei, Wenyu Liu, Qi Tian, and Xinggang Wang. 4d gaussian splatting for real-time dynamic scene rendering, 2024. URL <https://arxiv.org/abs/2310.08528>.
- Linning Xu, Vasu Agrawal, William Laney, Tony Garcia, Aayush Bansal, Changil Kim, Samuel Rota Bulò, Lorenzo Porzi, Peter Kontschieder, Aljaž Božič, et al. Vr-nerf: High-fidelity virtualized walkable spaces. In *SIGGRAPH Asia 2023 Conference Papers*, pp. 1–12, 2023.
- Chi Yan, Delin Qu, Dan Xu, Bin Zhao, Zhigang Wang, Dong Wang, and Xuelong Li. Gs-slam: Dense visual slam with 3d gaussian splatting. In *Proceedings of the IEEE/CVF Conference on Computer Vision and Pattern Recognition*, pp. 19595–19604, 2024.
- Zeyu Yang, Hongye Yang, Zijie Pan, and Li Zhang. Real-time photorealistic dynamic scene representation and rendering with 4d gaussian splatting, 2024. URL <https://arxiv.org/abs/2310.10642>.
- Ziyi Yang, Xinyu Gao, Wen Zhou, Shaohui Jiao, Yuqing Zhang, and Xiaogang Jin. Deformable 3d gaussians for high-fidelity monocular dynamic scene reconstruction, 2023. URL <https://arxiv.org/abs/2309.13101>.
- Zehao Yu, Anpei Chen, Binbin Huang, Torsten Sattler, and Andreas Geiger. Mip-splatting: Alias-free 3d gaussian splatting. In *Proceedings of the IEEE/CVF conference on computer vision and pattern recognition*, pp. 19447–19456, 2024.
- Yuheng Yuan, Qihong Shen, Xingyi Yang, and Xinchao Wang. 1000+ fps 4d gaussian splatting for dynamic scene rendering, 2025. URL <https://arxiv.org/abs/2503.16422>.
- Xinjie Zhang, Zhening Liu, Yifan Zhang, Xingtong Ge, Dailan He, Tongda Xu, Yan Wang, Zehong Lin, Shuicheng Yan, and Jun Zhang. Mega: Memory-efficient 4d gaussian splatting for dynamic scenes, 2025. URL <https://arxiv.org/abs/2410.13613>.
- Xiaoyu Zhou, Zhiwei Lin, Xiaojun Shan, Yongtao Wang, Deqing Sun, and Ming-Hsuan Yang. Drivinggaussian: Composite gaussian splatting for surrounding dynamic autonomous driving scenes, 2024. URL <https://arxiv.org/abs/2312.07920>.

A APPENDIX

A.1 USING LLM FOR POLISHING WRITING

We made limited use of a large language model (LLM) to assist with paper preparation, specifically for refining wording, improving clarity, and providing light proofreading. Its role was restricted to suggesting alternative phrasings and correcting minor grammatical issues, while all technical content and substantive writing were carried out by the authors. As this partial assistance helped improve readability and logical flow, we disclose it here in accordance with the ICLR policy.

A.2 ADDITIONAL IMPLEMENTATION DETAILS

In this section, we describe the implementation details and experimental settings in detail. As mentioned, we follow the Sub-Vector Quantization (SVQ) setup of OMG (Lee et al., 2025b), where codebook size of scale b_s , rotation b_r , and encoded appearance feature b_f are 2^9 , 2^{13} , and 2^{10} , respectively. Real-Time4DGS (Yang et al., 2024) introduces new attributes, s_t , scale along the time axis, and q^l , an additional quaternion to define the rotation matrix. We set their codebook size to 2^9 and 2^{13} , respectively. In terms of our small model (*Ours-S* and *Ours-T*), we decrease the size of the codebooks for 3D attributes to $b_s = 2^8$, $b_r = 2^{13}$, and $b_f = 2^{10}$, while keeping those for the two 4D attributes as they are. We set $\tau_{GS} = 0.4$ and $p = 0.8$ for *Ours-L*, while $\tau_{GS} = 0.3$ and $p = 0.9$ for *Ours-S* and *Ours-T*. We use the same codebook setup to both N3DV (Li et al., 2022b) and MPEG (Li et al., 2025) datasets. For MPEG (Li et al., 2025) dataset, we set $\tau_{GS} = 0.4$ and 0.6-quantile for *Ours-L* and 0.8-quantile for *Ours-S*.

For our FreeTimeGS (Wang et al., 2025a) experiment, we use $\tau_{GS} = 0.7$ and the quantile at level 0.6 for *Gaussian Pruning*, for the large model, while τ_{GS} is set to 0.3 and a 0.4-quantile is adopted for the small model, to aggressively prune the primitives. Similar to the Real-Time4DGS (Yang et al., 2024) implementation, we also sub-vector quantize the origin attributes that FreeTimeGS introduces, velocity and duration. We keep the identical codebook size for both scales of the model, and we use the codebook size 2^{10} for the velocity and duration.

A.3 ANALYSIS ON METHOD

SD Score. In this section, we analyze the proposed *SD* score in *Gaussian Sampling* stage. *Gaussian Sampling* aims to extract a subset of Gaussians that can faithfully represent both static and dynamic regions. Previous work (Oh et al., 2025) has attempted to leverage the variance of time distribution, Σ_t , as a cue to detect separate static and dynamic regions. Gaussians located at the regions with various motions tend to have relatively smaller values of Σ_t compared to those lying on the stationary area, as rapid changes in appearance or geometry restrict each primitive to have a short lifespan, being temporally localized. However, using Σ_t alone to select a subset with a limited budget can be biased toward extremes because sampling dynamic Gaussians by taking the bottom Σ_t subset focuses on a few high-velocity regions (e.g., moving hands in Fig. 6), while neglecting other dynamic structures such as secondary body motion. This is because Σ_t is agnostic to the visual contribution, oversampling transients that are temporally sharp. On the other hand, our *SD* Score addresses this by combining gradient-based contribution with temporal support. Under the same sampling budget, it can distribute the budget across multiple dynamic regions while keeping enough static structures, as shown in Fig. 6, producing better perceptual fidelity with the same number of Gaussians.

Gaussian Merging. Algorithm. 1 describes a detailed process of *Gaussian Merging*. As mentioned earlier, our *Gaussian Merging* performs correlation-considered Gaussian removal based on the locality of Gaussians, while *Gaussian Sampling* and *Gaussian Pruning* rather aim to identify the salience or contribution of a single Gaussian.

Ablation Studies. We further conduct ablation studies on the proposed method, evaluated on *cook spinach* and *sear steak* data of N3DV dataset (Li et al., 2022b). We compare each hyperparameter of the Gaussian removal stage. Tab. 5 and Tab. 6 show the comparison on different pruning ratio p and the number of *Gaussian Merging* implementation, respectively. As expected for Gaussian-

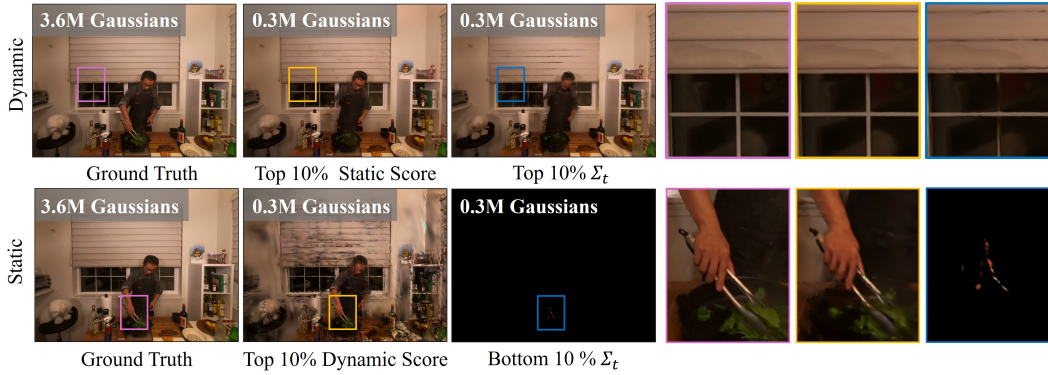


Figure 6: Effect of the sampling criterion under a fixed sampling budget. (Left) Rendered images with the full model. (Middle): Our *SD* Score selection using top 10% Static score and Dynamic Score. (Right) Σ_t -based sampling with the same sampling ratio.

Algorithm 1 Gaussian Merging

Require: Gaussian set \mathcal{P}_{GP} ; clusters $\mathcal{C} = \{C_q\}_{q=1}^{N_C}$; training steps T_M

Initialize per-member logits $\ell_i^x \leftarrow 0$, $\ell_i^f \leftarrow 0$ for all i

for $t = 1$ **to** T_M **do**

for all clusters C_q **do**

$$w_i^x \leftarrow \sigma(\ell_i^x) / \sum_{j \in C_q} \sigma(\ell_j^x) \quad \text{for } i \in C_q \quad \triangleright \text{Position weights}$$

$$w_i^f \leftarrow \sigma(\ell_i^f) / \sum_{j \in C_q} \sigma(\ell_j^f) \quad \text{for } i \in C_q \quad \triangleright \text{Appearance weights}$$

$$\bar{x}_q \leftarrow \sum_{i \in C_q} w_i^x x_i; \quad \bar{f}_q \leftarrow \sum_{i \in C_q} w_i^f f_i$$

$$\bar{a}_q \leftarrow a_{r(C_q)}, \quad r(C_q) = \arg \max_{i \in C_q} w_i^x$$

end for

$$\mathcal{P}_{\text{proxy}} \leftarrow \{(\bar{x}_q, \bar{f}_q, \bar{a}_q)\}_{q=1}^{N_C} \cup \{(x_i, f_i, a_i) : i \notin \bigcup_q C_q\}$$

 Render $\mathcal{P}_{\text{proxy}}$, compute loss \mathcal{L} , and update $\{\ell_i^x, \ell_i^f\}$ by backprop

end for

return pruned set $\mathcal{P}_{\text{proxy}}$

based models, the reconstruction quality increases monotonically with the number of Gaussians. We experimentally set these hyperparameters, considering the storage and image fidelity tradeoff.

Table 5: Ablation study on the quantile level of p of *Gaussian Pruning*.

Methods	PSNR \uparrow	SSIM \uparrow	LPIPS \downarrow	# Gaussians \downarrow	Storage (MB) \downarrow
$p = 0.6$	33.51	0.956	0.045	225,286	4.65
$p = 0.7$	33.47	0.956	0.046	172,193	3.95
$p = 0.8$	33.40	0.955	0.048	143,030	3.07
$p = 0.9$	33.05	0.950	0.055	83,052	1.91

A.4 PER-SCENE RESULTS

In this section, we provide per-scene results of the N3DV dataset (Li et al., 2022b) in Tab. 7. Qualitative results on N3DV (Li et al., 2022b) and MPEG (Li et al., 2025) are shown in Fig. 7 and Fig. 8, respectively.

Table 6: Ablation study on the number of *Gaussian Merging* execution M .

Methods	PSNR \uparrow	SSIM \uparrow	LPIPS \downarrow	# Gaussians \downarrow	Storage (MB) \downarrow
$M = 1$	33.44	0.955	0.047	161663	3.43
$M = 2$	33.40	0.955	0.048	143030	3.07
$M = 3$	33.32	0.954	0.049	130320	2.82
$M = 4$	33.26	0.954	0.0501	120347	2.63

Table 7: Quantitative results on N3DV (Li et al., 2022b) dataset. All results without * mark are sourced from the original paper. \dagger denotes post-processed models.

Method	Coffee Martini	Cook Spinach	Cut Roasted Beef	Flame Salmon	Flame Steak	Sear Steak	Average
PSNR \uparrow							
HexPlane (Cao & Johnson, 2023)	-	32.04	32.54	29.47	32.08	32.38	-
Real-Time4DGS (Yang et al., 2024)*	27.92	33.58	33.96	28.72	33.96	33.61	31.96
STG (Li et al., 2024)	28.61	33.18	33.52	29.48	33.64	33.89	32.05
4DGS (Wu et al., 2024)	27.34	32.46	32.90	29.20	32.51	32.49	31.15
MEGA (Zhang et al., 2025)	27.84	33.08	33.58	28.48	32.27	33.67	31.49
ADC-GS (Huang et al., 2025)-L	-	32.34	31.88	29.01	32.65	32.48	-
GIFStream (Li et al., 2025)	28.14	33.03	33.19	28.51	33.76	33.83	31.75
Ours-L	28.51	33.46	33.97	28.66	33.57	33.72	31.98
Ours-M	28.10	33.12	33.61	28.70	33.57	33.69	31.80
Ours-S	27.98	32.93	33.30	28.40	33.42	33.56	31.60
Ours-T	27.89	32.99	33.46	28.12	33.11	33.23	31.47
SSIM \uparrow							
HexPlane (Cao & Johnson, 2023)	-	-	-	-	-	-	-
Real-Time4DGS (Yang et al., 2024)*	0.915	0.957	0.960	0.921	0.962	0.961	0.946
STG (Li et al., 2024)	-	-	-	-	-	-	-
4DGS (Wu et al., 2024)	0.905	0.949	0.957	0.917	0.954	0.957	0.939
MEGA (Zhang et al., 2025)	-	-	-	-	-	-	-
ADC-GS (Huang et al., 2025)	-	-	-	-	-	-	-
GIFStream (Li et al., 2025)	0.905	0.950	0.947	0.916	0.957	0.958	0.938
Ours-L	0.913	0.953	0.955	0.916	0.960	0.960	0.943
Ours-M	0.910	0.952	0.954	0.916	0.958	0.958	0.941
Ours-S	0.907	0.950	0.950	0.086	0.956	0.956	0.939
Ours-T	0.906	0.949	0.950	0.912	0.955	0.955	0.934
LPIPS \downarrow							
HexPlane (Cao & Johnson, 2023)	-	0.082	0.080	0.078	0.066	0.070	-
Real-Time4DGS (Yang et al., 2024)*	0.077	0.040	0.037	0.070	0.038	0.041	0.051
STG (Li et al., 2024)	0.069	0.037	0.036	0.063	0.029	0.030	0.044
4DGS (Wu et al., 2024)	-	-	-	-	-	-	-
MEGA (Zhang et al., 2025)	0.077	0.047	0.048	0.073	0.053	0.040	0.056
ADC-GS (Huang et al., 2025)	-	-	-	-	-	-	-
GIFStream (Li et al., 2025)	-	-	-	-	-	-	-
Ours-L	0.082	0.047	0.045	0.078	0.042	0.042	0.056
Ours-M	0.085	0.049	0.049	0.080	0.458	0.458	0.059
Ours-S	0.091	0.054	0.055	0.086	0.049	0.049	0.064
Ours-T	0.092	0.057	0.058	0.088	0.052	0.054	0.067
# Gaussians \downarrow							
Real-Time4DGS (Yang et al., 2024)*	4,644,826	3,612,582	2,990,635	4,844,269	2,371,722	1,921,026	3,397,510
Ours-L	379,416	297,478	274,566	354,320	209,592	184,411	283,297
Ours-M	229,077	179,852	167,268	220,867	123,546	106,208	171,136
Ours-S	184,365	138,963	134,193	175,395	102,712	88,858	137,414
Ours-T	151,908	113,542	106,171	142,625	82,987	71,179	111,402
Storage (MB) \downarrow							
Real-Time4DGS (Yang et al., 2024)*	2852	2218	1836	2975	1456	1179	2086
Ours-L	7.54	6.04	5.61	7.1	4.36	3.87	5.75
Ours-M	4.71	3.78	3.54	4.56	2.69	2.36	3.61
Ours-S	3.32	2.57	2.49	3.17	1.95	1.71	2.54
Ours-T	2.77	2.13	2.01	2.62	1.61	1.41	2.09

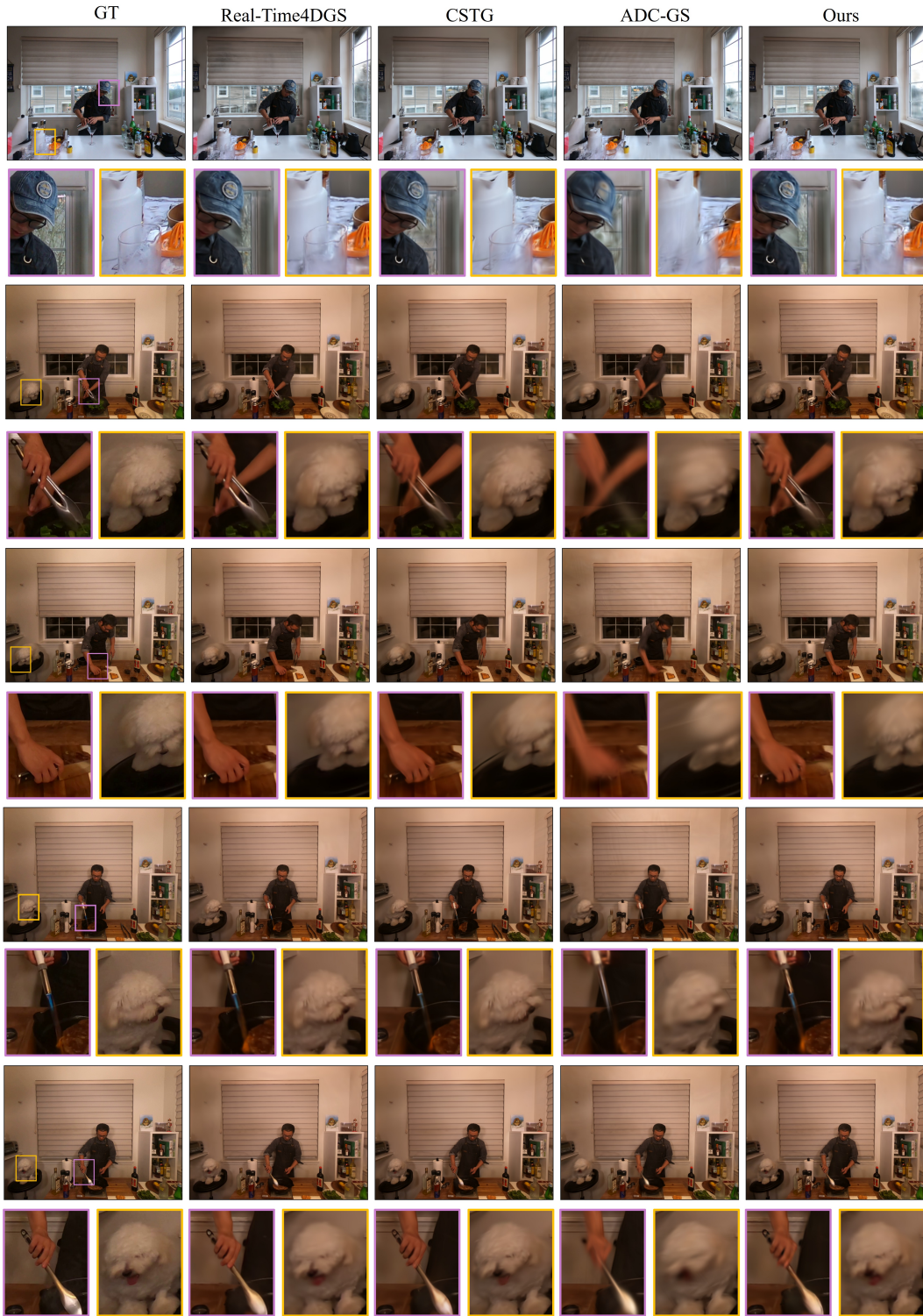


Figure 7: Additional qualitative results on N3DV (Li et al., 2022b) dataset.

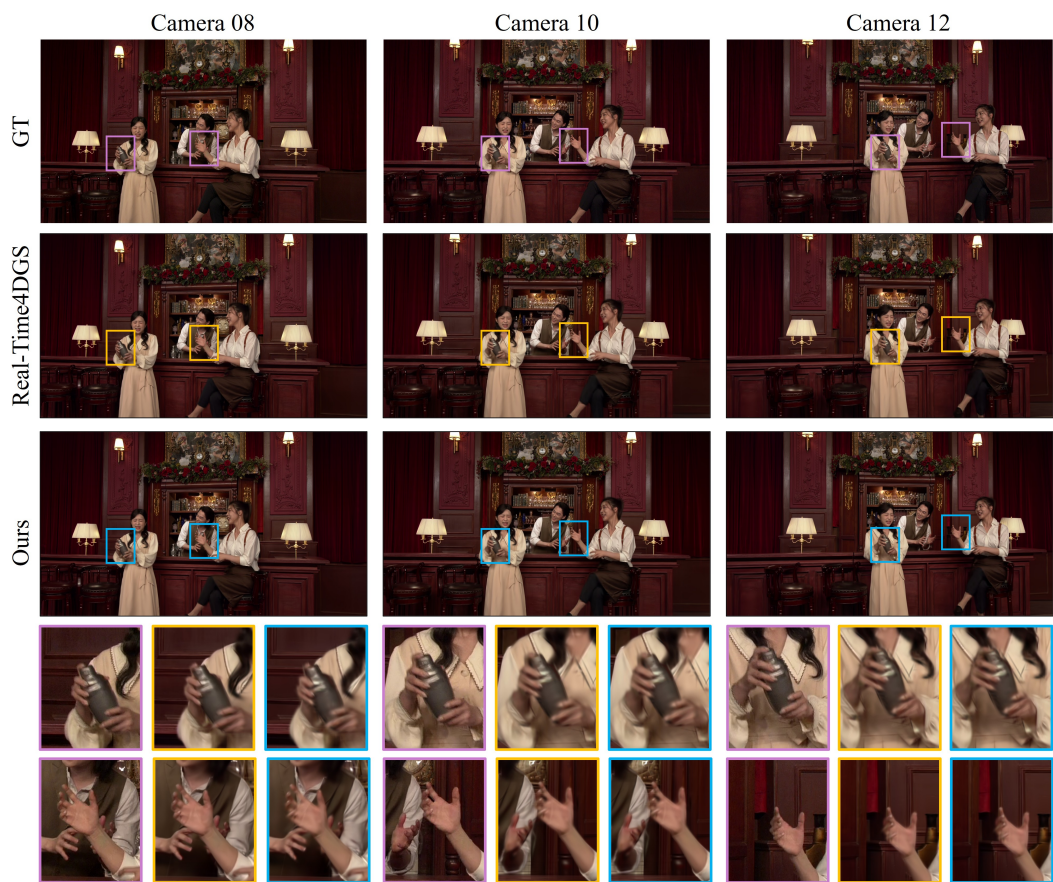


Figure 8: Qualitative results on MPEG (Li et al., 2025) dataset.